Automated Negative Lightning Return Strokes Characterization Using Brute-Force Search Algorithm

Faranadia Abdul Haris[1,2]*, Mohd Zainal Abidin Ab. Kadir[1], Sukhairi Sudin[3], Jasronita Jasni[1], Dalina Johari[2] and Nur Hazirah Zaini[4]

[1]*Advanced Lightning, Power and Energy Research (ALPER), Faculty of Engineering, Universiti Putra Malaysia, 43400 UPM, Serdang, Selangor, Malaysia*
[2]*School of Electrical, College of Engineering, Universiti Teknologi MARA, 40450 UiTM, Shah Alam, Selangor, Malaysia*
[3]*Faculty of Electrical Engineering Technology, Universiti Malaysia Perlis, 02600 UniMAP, Arau, Perlis, Malaysia*
[4]*Faculty of Engineering and Built Environment, Universiti Sains Islam Malaysia, 71800 USIM, Bandar Baru Nilai, Nilai, Negeri Sembilan, Malaysia*

ABSTRACT

Over the years, many studies have been conducted to measure, analyze, and characterize the lightning electric field waveform for a better conception of the lightning phenomenon. Moreover, the characterization mainly on the negative return strokes also significantly contributed to the development of the lightning detection system. Those studies mostly performed the characterization using a conventional method based on manual observations. Nevertheless, this method could compromise the accuracy of data analysis due to human error. Moreover, a longer processing time would be required to analyze data, especially for larger sample sizes. Hence, this study proposed the development of an automated negative lightning return strokes characterization using a brute-force search algorithm. A total of 170 lightning electric field waveforms were characterized automatically using the proposed algorithm. The manual and automated data were compared by evaluating their percentage difference, arithmetic mean (AM), and standard deviation (SD). The statistical analysis showed a good agreement between the manual and automated data with a percentage difference of 1.19% to 4.82%. The results showed that the proposed algorithm could provide an

E-mail addresses:
faranadia@uitm.edu.my (Faranadia Abdul Haris)
mzk@upm.edu.my (Mohd Zainal Abidin Ab. Kadir)
sukhairi@unimap.edu.my (Sukhairi Sudin)
jas@upm.edu.my (Jasronita Jasni)
dalinaj@uitm.edu.my (Dalina Johari)
nurhazirah@usim.edu.my (Nur Hazirah Zaini)
* Corresponding author

efficient structure and procedure by reducing the processing time and minimizing human error. Non-uniformity among users during negative lightning return strokes characterization can also be eliminated.

INTRODUCTION

In the lightning phenomenon, the overall effect of lightning is called a flash, in which the lightning flash consists of several strokes. The lightning strike can be defined as a lightning flash where the lightning-generated electric fields in the thundercloud are typically 100–200 kW/m and can be as high as 400 kV/m. The mechanism of ground flash involves many physical processes such as preliminary breakdown, stepped leaders, connecting leaders, return strokes, and subsequent return strokes (Cooray, 2014). The most common downward ground flash is a negative ground flash initiated by a lower negative charge region from the thundercloud to the ground. The preliminary breakdown process refers to initiating an electrical breakdown inside the thundercloud, which consists of multitudes of discharges that lead to the development of a leader that propagates in a stepped structure towards the ground (Dwyer & Uman, 2014).

Meanwhile, the return stroke is a luminosity event that travels upward one-third of the speed of light in free space, approximately $1x10^8$ m/s (Idone & Orville, 1982). This event happens when the connection between the stepped leader and ground has been made, and a wave of near-ground potential travels along the leader channel toward the cloud (Cooray, 2015). This cloud-to-ground lightning flash typically lasts for 0.5 seconds, usually composed of several intermittent discharges called strokes having a duration of milliseconds each (Rakov, 2016). The sudden flow of electric charge out of the channel and into the striking point will generate a large current, which the average peak of current can be as high as 30 kA with each of the strikes could initiate 80 kA or more. As a return stroke rises, heat will be generated where the temperature of the air in the discharge channel can reach 30,000 K in a few microseconds (Orville, 1968). This temperature is six times higher than the Sun's surface, approximately 5,778 K.

Generally, previous studies widely used a parallel-plate antenna to conduct lightning measurement, mainly on the electric field measurement (Cooray & Lundquist, 1982; Gomes et al., 1998; Sharma et al., 2005; Cooray & Lundquist, 1985; Ibrahim et al., 2011; Hamzah, 2015). Based on the measurement setup, the lightning electric field events were recorded using a specific transient recorder system, for example, Tektronix, PiscoScope, Yokogawa, or any other data logger system. All the recorded waveforms were commonly used for characterization and further analysis based on the manual observations. From these observations, it was important to classify the electric field change of the recorded waveform by identifying the sign convention. A positive signal which occurred when there

was an upward curve from the recorded waveform, corresponded to the negative charges being lowered to the ground and vice versa, according to the atmospheric sign convention (Cooray, 2003; Gomes et al., 2013; Haddad et al., 2012; Nag & Rakov, 2014). Therefore, a positive electric field change in a waveform indicated negative return strokes. Further, the atmospheric sign convention was applied in most previous studies compared to the physics sign convention, which contradicts the atmospheric sign convention (Beasley, 1985).

Based on the reviewed studies, it was found that the characterization and analysis made mainly on the negative return strokes were performed mostly by adopting manual observation on every frame of the recorded waveform/data (Ahmad et al., 2010; Hazmi et al., 2017; Heidler & Hopf, 1998; Hojo et al., 1985; Ishii & Hojo, 1989; Master et al., 1984; Santamaría et al., 2006; Weidman & Krider, 1978; Wooi et al., 2016). In contrast, an automated negative lightning return strokes characterization using the brute-force search algorithm, including its concept details and operation, is proposed in this study. The brute force search algorithm is one of the basic local search methods in computer science. This algorithm has been applied in this study because of the working principle that will visit each waveform point without pruning any point. In contrast with the minimax algorithm, it will cut certain points of the searching tree. The minimax depends on the available score, making not all waveform points visited by the algorithm. Meanwhile, the hill-climbing search algorithm can drive to state which it is commonly get stuck by local optimum. In this case, the algorithm has the potential to go back to the original point without searching for a new point (Sudin, 2019). Hence, seven negative return stroke parameters were characterized using the brute-force search algorithm. In addition, the manually characterized data and the automated data from the proposed algorithm were also compared and analyzed. The remainder of this paper is structured as follows: Section 2 presents the approach by describing the data characterization and processing framework; Section 3 discusses the results, and Section 4 concludes the study results.

METHODS

Automated Negative Lightning Return Strokes Characterization

Figure 1 illustrates the steps involved in the proposed automated negative lightning return strokes characterization developed in this study. First, the raw data of the measured waveform/signal were fetched from the transient recorder system. The transient recorder systems used in this study were Picoscope Series 4000. The PicoScope 4000 series is usually supplied with the PicoScope software, which can be installed on a personal computer (PC) with operating system requirement of Windows XP SP2 or Vista (32- bit versions), convenient for the large display, storage, user interface, and networking built in the particular PC. This 12-bit oscilloscope is composed of BNC (Bayonet Neill–Concelman) type connectors whose inputs have an impedance of 1 MΩ that is compatible with all

standard scope probes, including x1, x10, and switched types. In addition, the rear panel is composed of a USB 2.0 port connected to the PC, which offered a highly portable oscilloscope since there was no requirement of an external power supply as power was supplied from the USB port. A full spectrum of the raw data was then plotted to find its peak amplitude. If the peak amplitude was observed in positive value (+ve), the signal was recognized as negative return strokes.

In contrast, if the peak amplitude was identified in negative value (-ve), the signal was classified as positive return strokes. The proposed algorithm did not process the positive return strokes at the next stage (to find the other parameters such as zero-to-peak rise time, zero-crossing time, and fast transition time), as shown in Figure 2. Therefore, for this case, the proposed algorithm will classify the positive return strokes as others because this study only focused on the negative return strokes. It is because positive lightning is less common
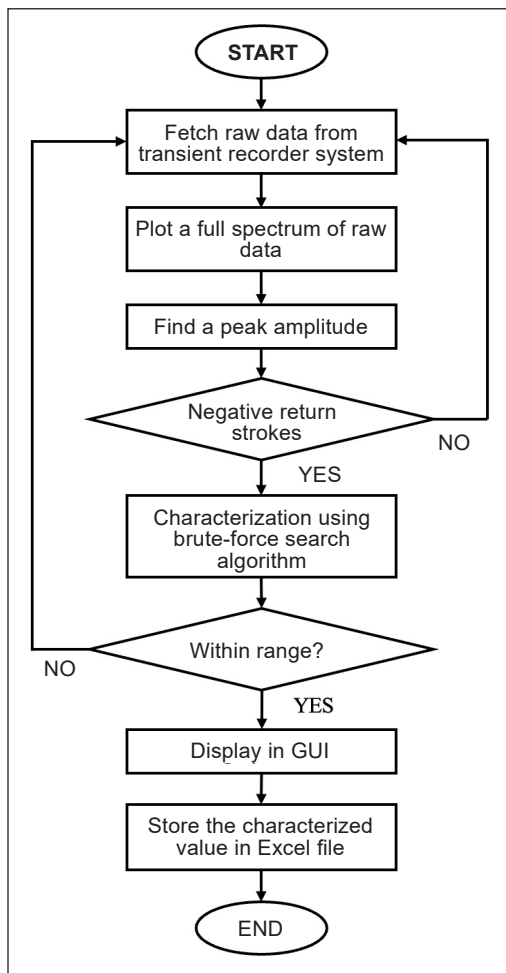

Figure 1. Flow chart of the proposed automated negative lightning return strokes characterization
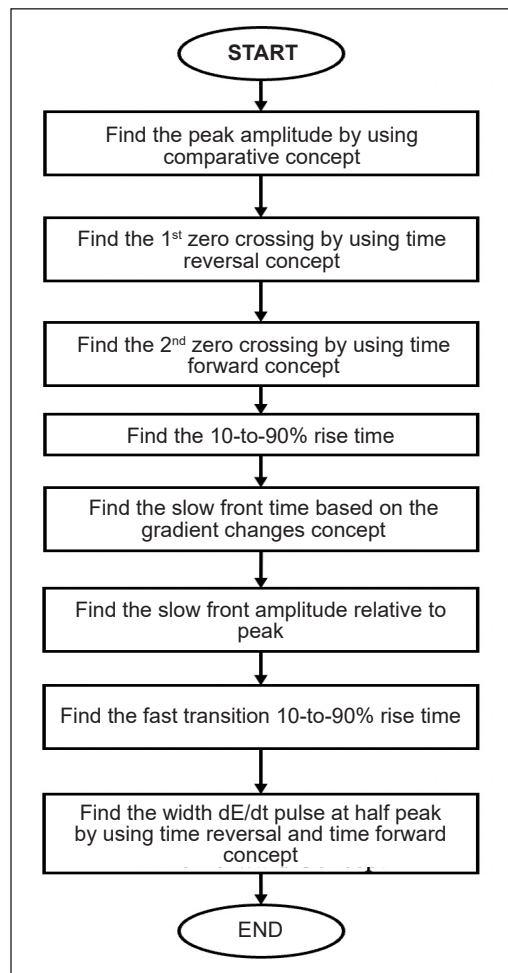

Figure 2. Flow chart of the proposed brute-force search algorithm

than negative lightning, which the measured data of the positive return stroke is much lower than the negative return stroke. The measured data in this study is also agreeable with the previous research conducted in a tropical region, in which the negative return stroke was the region's most prevalent lightning compared to the positive return stroke (Chi et al., 2014).

At the next stage, all the parameters of the negative return strokes characterized by the brute-force search algorithm were plotted using MATLAB software (version 2018b (9.5.0.94444). Each of the values obtained from this algorithm was then compared with the range of negative return stroke parameters defined from the previous study conducted at Universiti Putra Malaysia, corresponding to tropical climate variation (Arshad, 2017). The data were then displayed via a Graphic User Interface (GUI) as negative return strokes for parameters within range. Additionally, all the raw data synthesized from the proposed algorithm were stored in excel file format (*.xlsx).

Brute-Force Search Algorithm

The brute-force algorithm is an exhaustive search algorithm that previous studies have adopted for characterization and classification (Cikač et al., 2020; Davidrajuh & Rong, 2019; Klaver et al., 2018; Raafat & Naji, 2018; Sudin, 2019; Thike et al., 2017). This algorithm provides an effective method to determine an optimal solution by identifying all the possible combinations, and each combination is examined one after another (Chum et al., 2014; Robinson & Quinn, 2018). Figure 2 illustrates the flow chart of the proposed brute-force search algorithm. In this study, the proposed brute-force search algorithm was operated by applying several search concepts such as comparative, time reversal, and time forward. The proposed algorithm also worked based on the criteria defined by this study. Specifically, the criteria for each parameter of negative return strokes were defined and interpreted based on the mathematical equations highlighted next. Seven parameters of negative return strokes were involved in this study: (1) zero-to-peak rise rime; (2) 10-to-90% rise time; (3) zero-crossing time; (4) slow front time; (5) slow front amplitude relative to peak; (6) fast transition 10-to-90% rise time, and (7) width dE/dt pulse at half peak (Wooi et al., 2016; Arshad, 2017). Figure 3 presents the parameters of negative return strokes.
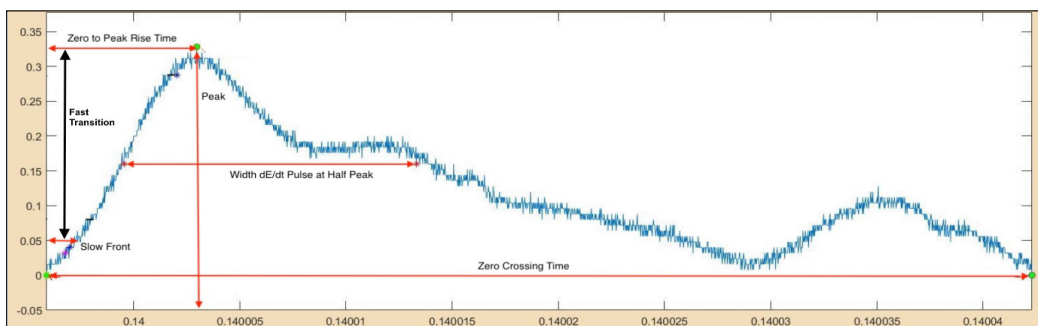

Figure 3. Parameters of negative return strokes

As shown by the flow chart in Figure 2, the first step was identifying the time at the peak amplitude, referred to as t_p. Through the proposed algorithm, t_p was determined using a comparative concept where the value of each raw data was compared to find a maximum value of amplitude. In this study, a_n is the amplitude value at point zero, while a_{n+1} is the amplitude value at any point other than zero. When the value of point a_n is less than a_{n+1}, the peak (P) is equal to a_{n+1}, which was how the comparative concept worked. After that, the looping process continued until the value of a_n was greater than a_{n+1}. Eventually, the highest amplitude value (a_n) became the peak value (P). Figure 4 shows a flowchart of the simplified pseudocode.

The zero-to-peak rise time (t_{z1p}) was defined based on Equation 1:

$$t_{z1p} = t_p - t_{z1} \qquad (1)$$

Figure 4. Flow chart of the simplified pseudocode for peak amplitude

where t_p is the time at the peak magnitude, and t_{z1} is at the first zero-crossing. The value for t_{z1p} was obtained by subtracting t_p with t_{z1}. It was also determined using the time-reversal concept, which can be seen from the flow chart in Figure 2. Based on this concept, the time was reversed from a starting point which was from the t_p, where the amplitude on each time was observed. This process was continued until the time where the amplitude was equal to zero was found, which corresponded to t_{z1}.

Meanwhile, the zero-crossing time (t_z) was defined using Equation 2:

$$t_z = t_{z2} - t_{z1} \qquad (2)$$

where t_{z2} is the time at the second zero-crossing, and t_{z1} is first. The zero-crossing time can be defined as the first at the rising time (t_{z1}) and the second at fall time (t_{z2}). The time's starting point determined the first and second zero-crossings times at the peak amplitude (t_p). A time forward concept was implemented to find the second zero-crossing time (t_{z2}) for this parameter. By taking a starting point of time at the peak amplitude (t_p), the proposed algorithm searched and moved forward until it detected the time where the amplitude was
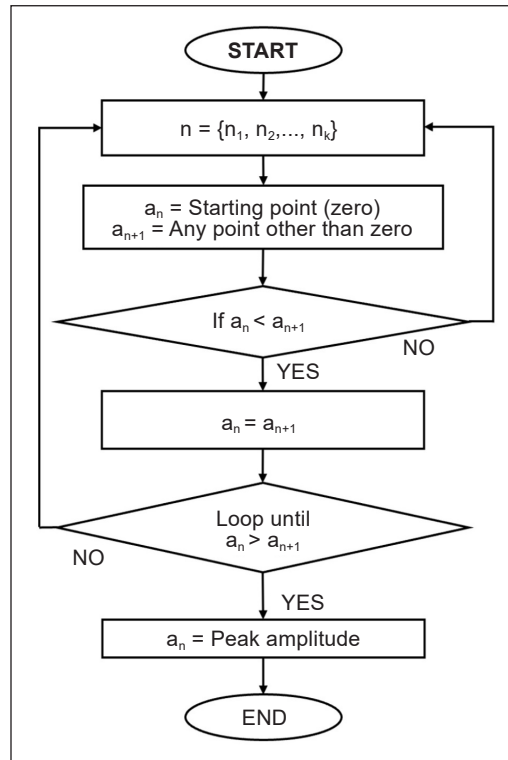
equal to zero, referred to as t_{z2}. Meanwhile, the first zero-crossing time (t_{z1}) was identified in the previous step using the time-reversal concept.

Next, the 10-to-90% rise time was defined based on Equation 3:

$$t_{r10-90} = t_{r90} - t_{r10} \tag{3}$$

where t_{r90} is the time at 90% of the zero-to-peak amplitude, and t_{r10} is at 10% of the zero-to-peak amplitude. The value for t_{r10-90} was obtained by subtracting t_{r90} with t_{r10}.

Furthermore, the 10% and 90% of zero-to-peak amplitudes were constructed by using Equations 4 and 5:

$$10\% \; of \; zero - to - peak \; amplitude = (0.1) \times (P) \tag{4}$$

$$90\% \; of \; zero - to - peak \; amplitude = (0.9) \times (P) \tag{5}$$

where P is the waveform peak amplitude, the time at 10% of the zero-to-peak amplitude (t_{r10}) was determined by identifying the time at which the amplitude approached 10% of the zero-to-peak amplitude. In contrast, the time at 90% of the zero-to-peak amplitude (t_{r90}) was determined when the time reached 90% of the zero-to-peak amplitude.

The slow front duration was determined based on the gradient changes from the zero-to-peak amplitude. In this study, the slow front's gradient angle was set to equal and less than 45°. The gradient (m) and angle (θ) were constructed using Equations 6 and 7:

$$m = \frac{y_2 - y_1}{x_2 - x_1} \tag{6}$$

$$\theta = tan^{-1} m \tag{7}$$

where y is the waveform amplitude (E), and x is the time (t). The algorithm worked based on the criteria defined from Equation 7. In this process, the algorithm searched and compared at least ten points from the vertical and horizontal axis to find the gradient (m) as well as the angle (θ), starting from the first zero-crossing until the zero-to-peak (rise time region). The slow front time (t_{sf}) was obtained when θ was observed greater than 45° based on the intersection point of the plotted gradients, as depicted in Figure 5. In this case, the 45^0 is the turning point between the maximum time of the slow front occurrence and the fast transition occurrence. Hence, the t_{sf} can be determined based on the difference between the maximum time of the slow front occurrence with the first zero-crossing time. Based on the previous study, the 'break point' or 'turning point' between the slow front and the fast transition has been identified from the naked eye on the recorded electric field waveform. However, no standard guideline (in terms of angle's value) has been highlighted to identify

the turning point (Willet & Krider, 2000; Hamzah, 2015; Wooi et al., 2016; Arshad, 2017). Hence, this study proposed the turning point between the slow front and fast transition at an angle of 45°. When the angle is greater than 45°, the waveform becomes quite steep, which is uncommon for a slow front occurs at that particular angle from the manual observation.

The slow front amplitude relative to peak value is given by Equation 8:

$$Slow\ front\ amplitude\ relative\ to\ peak = \frac{P_{sf}}{P} \times 100 \qquad (8)$$

where P_{sf} is the slow front amplitude and is P the waveform peak amplitude, the slow front amplitude relative to peak value was determined based on the ratio between P_{sf} with P. In this part, after the maximum time of the slow front occurrence (t_{sf}) has been obtained, the amplitude can be determined from the y-axis (E). Hence, the value of the y-axis at the maximum time of the slow front occurrence can be represented as the slow front amplitude (P_{sf}), as shown in Figure 5.

The fast transition occurs between peak amplitude (t_p) and the slow front (t_{sf}) time. Hence, the fast transition 10-to-90% rise time was defined using the following Equation 9:

$$t_{f10-90} = t_{f90} - t_{f10} \qquad (9)$$

Where t_{f90} is the time at 90% of the fast transition amplitude, and t_{f10} is at 10% of the fast transition amplitude, as shown in Figure 6. In this part, the fast transition amplitudes are identified by subtracting the peak amplitude (P) with the slow front amplitude (P_{sf}). Since the fast transition occurs after the slow front region, the fast transition amplitude was taken
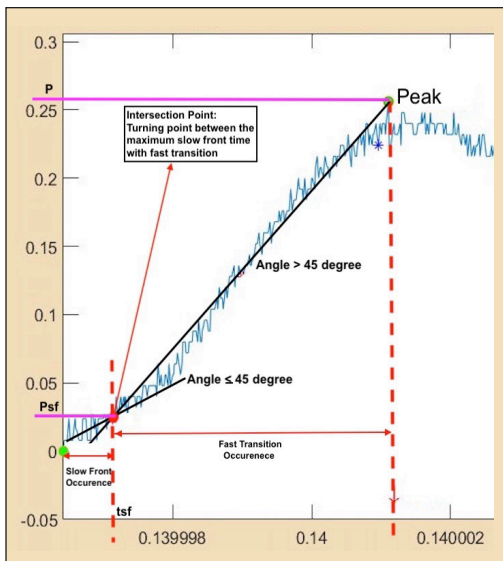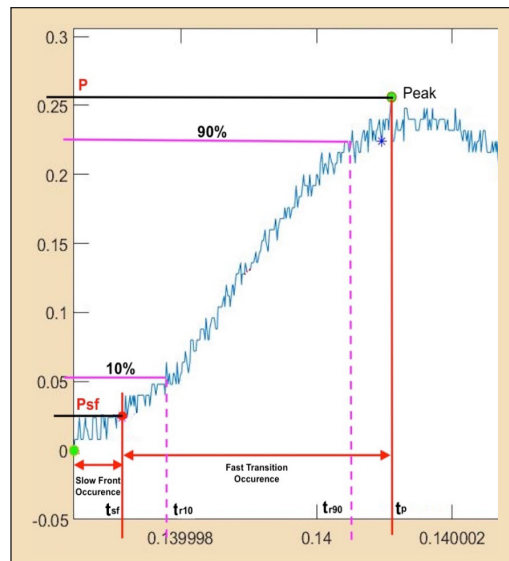

Figure 5. Slow front time

Figure 6. Fast transition 10-90% rise time

from the starting point at Psf. Therefore, 90% and 10% of the fast transition amplitude criteria were constructed using Equations 10 and 11, respectively.

$$90\% \; of \; fast \; transition \; amplitude \; = \; [(P - P_{sf}) \times (0.9)] \; + \; P_{sf} \quad (10)$$

$$10\% \; of \; fast \; transition \; amplitude \; = \; [(P - P_{sf}) \times (0.1)] \; + \; P_{sf} \quad (11)$$

The half peak amplitude (HPA) and the width of dE/dt pulse at half peak value (t_{hp}) were defined using given Equations 12 and 13:

$$HPA = \frac{P}{2} \tag{12}$$

$$t_{hp} = t_f - t_r \tag{13}$$

where p is the waveform peak amplitude, t_f is the fall time at HPA, and t_r is the rise time at HPA. As shown by Equation 12, the HPA was obtained by dividing the peak amplitude in half. Meanwhile, tr was identified using a reversal time concept, where the time was reversed until the time at HPA was detected, referred to as t_r. In contrast, t_{hp} was calculated by subtracting t_f with t_r. Apart from that, t_f was determined using a time forward concept, where the time moved forward from a starting point from the peak amplitude (t_p). This process was continued until the time at HPA was found, which corresponded to t_f.

Evaluation of Performance

The percentage difference between manual and automated data was calculated to compare automated performance across a different range of data involved by observing how close the automated data was to the manual data. The percentage difference is given from Equation 14 (Hyndman & Koehler, 2006);

$$Percentage \; Difference \; (\%) = \sum \left(\frac{automated - manual}{manual} \right) \times 100\% \quad (14)$$

RESULTS AND DISCUSSIONS

In this study, 170 electric field waveforms were characterized by using the proposed algorithm. Table 1 shows the compared data between manual and automated for each parameter of the negative return strokes. The automated data were characterized automatically from the proposed algorithm. Meanwhile, the manual data were identified based on manual observation from the scope. The comparison was also analyzed using Bland-Altman plots that provided an effective method to validate the two different data measurements (Miller & Ranum, 2011).

Table 1
Summary of data comparison between manual and automated for negative return strokes

Parameters	Manual		Automated		Percentage Difference (%)
	AM	*SD*	*AM*	*SD*	
Zero-to-Peak Rise Time (μs)	6.7	2.57	6.62	2.53	1.19
10-to-90% Rise Time (μs)	4.51	1.25	4.31	1.36	4.43
Zero-Crossing Time (μs)	33.79	12.77	32.63	12.65	3.43
Slow Front Time (μs)	4.36	2.08	4.15	1.88	4.82
Slow Front Amplitude Relative to Peak (%)	28.8	8.46	28.27	8.35	1.84
Fast Transition 10-to-90% Rise Time (μs)	3.95	1.71	3.88	1.68	1.77
Width dE/dt Pulse at Half Peak (μs)	3.57	1.23	3.51	1.17	1.68

Note. AM: Arithmetic mean; SD: Standard deviation

A significant difference can be seen from Table 1 between the manual and automated data for the zero-to-peak rise time, in which the percentage difference was 1.19%. It is because the manual data were data based on manual observation. In contrast, the automated data were data characterized based on the criteria defined from Equation 1, in which the brute-force search algorithm employed a time-reversal concept. Based on Table 1, the comparison with the manual data revealed that the AM (6.62) and SD (2.53) of the automated data were slightly lower, particularly 1.19% and 1.56%, respectively. Apart from that, the Bland-Altman plot from Figure 7 presents the mean difference between the manual and automated data measurement with -0.0155 bias, corresponding to zero differences. For this parameter, the lower and upper limits were -1.04 and 1.07, respectively.

A noticeable difference can be seen between the manual and automated data for the zero-crossing time, in which the percentage difference was determined as 3.43%. The automated data were characterized based on the criteria of zero-crossing time from Equation 2, in which the brute-force search algorithm employed both time-reversal and time-forward
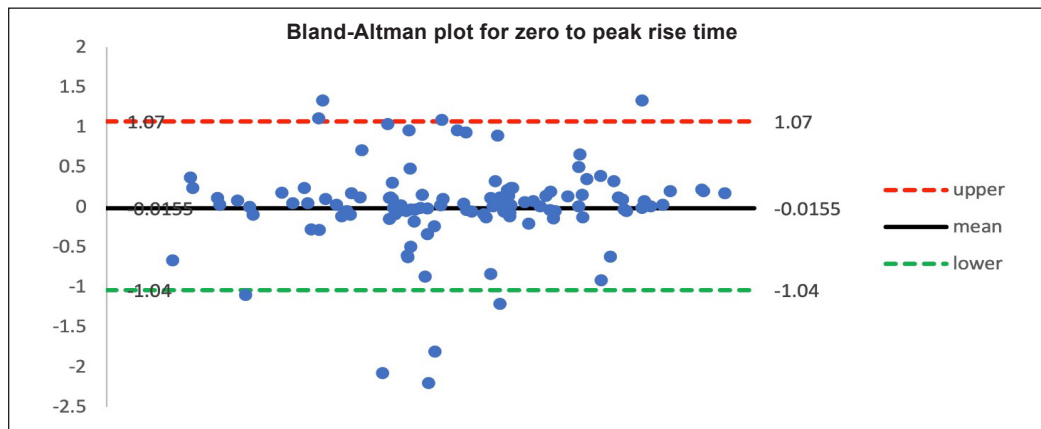

Figure 7. Bland-Altman plot for zero to peak rise time

concepts. Besides, there is a slight difference in AM and SD between the manual and automated data. Based on Table 1, the comparison with the manual data revealed that the AM (32.63) and SD (12.65) of the automated data were slightly lower, particularly 3.43% and 0.94%, respectively. In addition, Figure 8 shows the Bland-Altman analysis of zero-crossing time for both manual and automated data, through which the mean difference was determined as 0.2238, corresponding to zero differences. Meanwhile, the lower and upper limits were observed as -4.718 and 5.166, respectively.

Figure 8. Bland-Altman plot for zero crossing time

For the 10-to-90% rise time, a significant difference between the automated and manual data was observed with a calculated percentage difference of 4.43%. The automated data were characterized using the brute-force search algorithm based on the criteria defined from Equation 3. From Table 1, the AM of automated data (4.31) was found to be slightly lower (4.43%) than the manual data (4.51). On the contrary, the SD for automated data (1.36) was slightly higher (8.80%) than the manual data. As can be seen from Figure 9, the mean difference between the manual and automated data was discovered as 0.1313, which corresponded to zero differences. Furthermore, the associated lower and upper limits were observed as -0.59 and 0.86, respectively.

A noticeable difference can be seen for the slow front time, in which the percentage difference between manual and automated data was calculated as 4.82%. The automated data were characterized using the brute-force search algorithm according to the criteria defined from Equations 6 and 7, based on the intersection point of the plotted gradients. Based on Table 1, the comparison with the manual data revealed that the AM (4.15) and SD (1.88) of the automated data were slightly lower, particularly 4.82% and 9.62%, respectively. The automated data were slightly lower than the manual as the maximum angle of the slow front gradient might be higher or lower than the assumption value, thus resulting in the variance. The manual data for a slow front time was observed based on

the difference between the two slopes at the rise time signal. The slow front occurs before the fast front, in which the turning point between these two signals was estimated from the naked eye. Hence, the estimated turning point of the slow front's slope might differ from the automated approach that contributes to the highest percentage difference. Figure 10 shows that the mean difference between the manual and automated data was observed at 0.0833, corresponding to zero differences. Meanwhile, the lower and upper limits were observed as -0.93 and 1.09, respectively.

Based on Table 1, a significant difference between the manual and automated data can be seen for the slow front relative amplitude to the peak. The percentage difference was calculated as 1.84%. The criteria of slow front amplitude relative to peak were defined from Equation 8, where the slow front amplitude was divided by the waveform peak amplitude. The automated data were characterized using the brute-force search algorithm based on these established criteria. Further comparative analysis showed that the AM (28.27) and SD (8.35) for the automated data were slightly lower than the manual data, with a difference
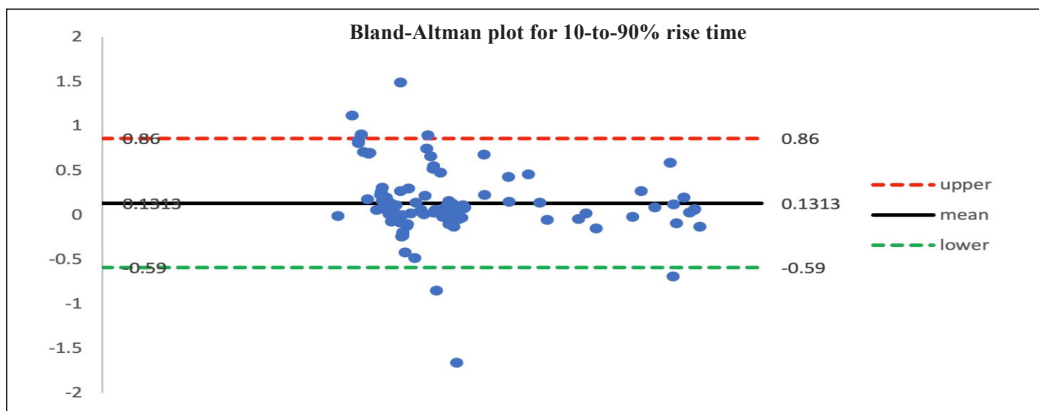

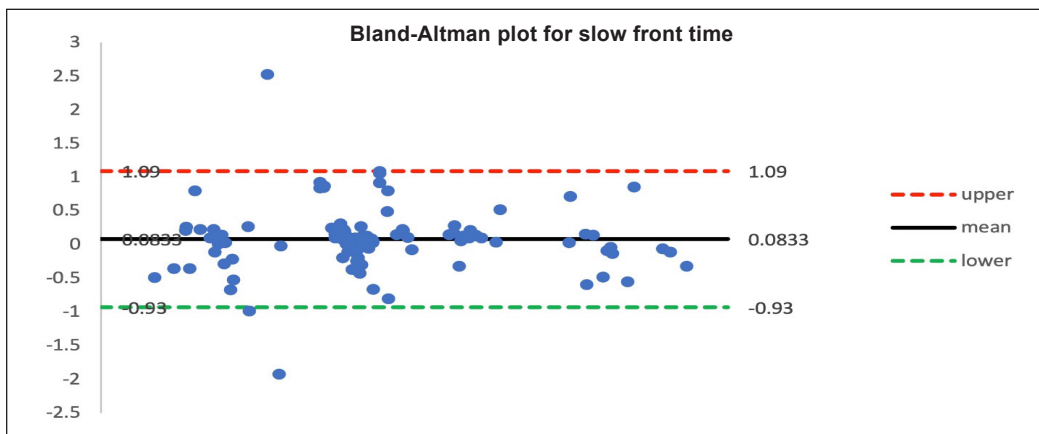*Figure 9*. Bland-Altman plot for 10-to-90% rise time

Figure 10. Bland-Altman plot for slow front time

of 1.84% and 1.30%, respectively. Besides, the Bland-Altman plot analysis in Figure 11 showed that the mean difference between the manual and automated data was observed as 0.1168, corresponding to zero differences. Furthermore, the lower and upper limits were observed as -2.73 and 2.97, respectively.

A significant difference can be seen between the manual and automated data for the fast transition 10-to-90% rise time, in which the percentage difference was calculated as 1.77%. The automated data was characterized using the brute-force search algorithm based on the criteria defined from Equation 11. The fast transition was taken between the time at peak amplitude with the slow front time. Apart from that, the comparative analysis showed that the AM of automated data (3.88) was slightly lower (1.77%) than the manual data (AM = 3.95). On the same note, the SD of automated data (1.68) was also slightly lower (1.75%) than the manual data (SD = 1.71). The Bland-Altman plot from Figure 12 illustrates the mean difference between the manual and automated data measurement with 0.0679 bias, corresponding to zero differences. Furthermore, the lower and upper limits were observed as -0.69 and 0.83, respectively.
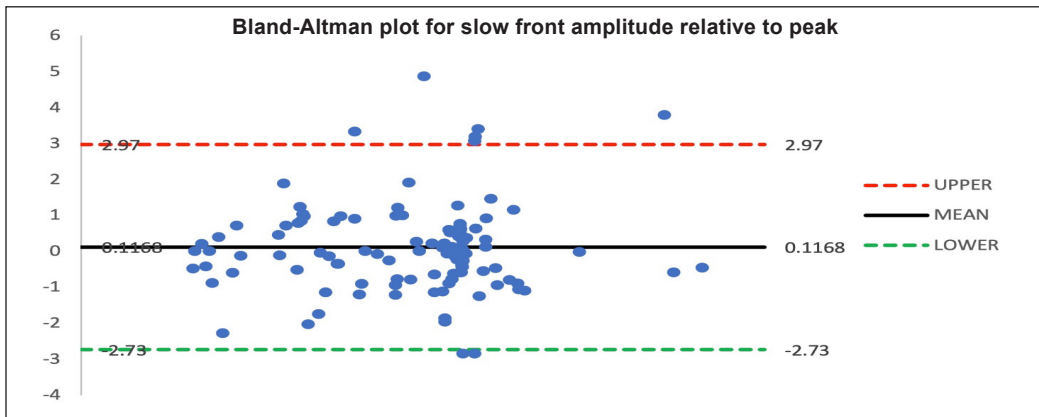

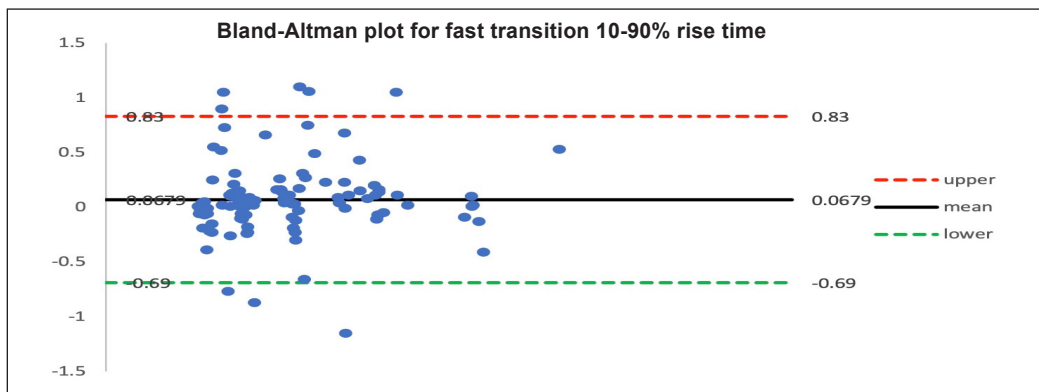*Figure 11*. Bland-Altman plot for slow front amplitude relative to peak

Figure 12. Bland-Altman plot for fast transition 10-90% rise time

A noticeable difference can be seen between the manual and automated data for width dE/dt pulse at half peak, in which the percentage difference was identified as 1.68%. The automated data were characterized based on Equation 13, which was constructed by implementing both the time-reversal and time-forward concepts. From Table 1, the comparison revealed that the AM of the automated data (3.51) was slightly lower (1.68%) than the manual data (AM = 3.57). Similarly, the SD of the automated data (1.17) was also slightly lower (4.88%) than the manual data (SD = 1.23). Besides, from Figure 13, the mean difference between the manual and automated was discovered as 0.0453, corresponding to zero differences. Furthermore, the lower and upper limits for the width dE/dt pulse at half peak value were observed as -0.43 and 0.52, respectively.

Overall, the differences between manual and automated data for all parameters are due to the algorithm's decimal places of each point/time calculated by the algorithm being much larger. Compared to the manual approach, all the points are observed and calculated in smaller decimal places which most of the value has been rounded up to one or two decimal places. The different number of decimal places taken could contribute to differences/variations in the results from the basic mathematical calculations. In addition, a non-uniformity of the value/point taken while characterizing the data manually also gives a significant contribution to differences with automated data. The automated data is based on the fixed structure that provides a proper/standard guideline and operation in the characterization algorithm based on the desired requirement defined from the developed mathematical equations. Hence, the difference between the non-uniformity data (manual approach) and the fixed structure (automated data) might also contribute to these differences.

Figure 14 illustrates the developed Graphic User Interface (GUI) for an automated approach by displaying a full spectrum lightning-generated electric waveform and characterizing the negative lightning return strokes through Matlab software. At the top,
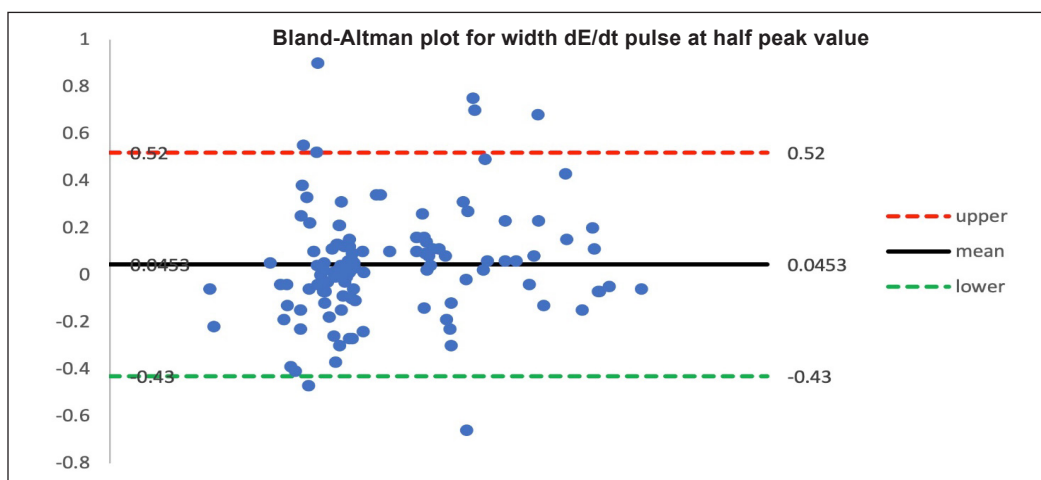

Figure 13. Bland-Altman plot for width dE/dt pulse at half peak value

the full spectrum of the raw data/output waveform fetched from the transient recorder system is displayed. While the negative return strokes that were characterized and analyzed automatically using the proposed brute-force search algorithm are illustrated in the second window. The value for each of the negative return stroke parameters is also presented in the GUI.
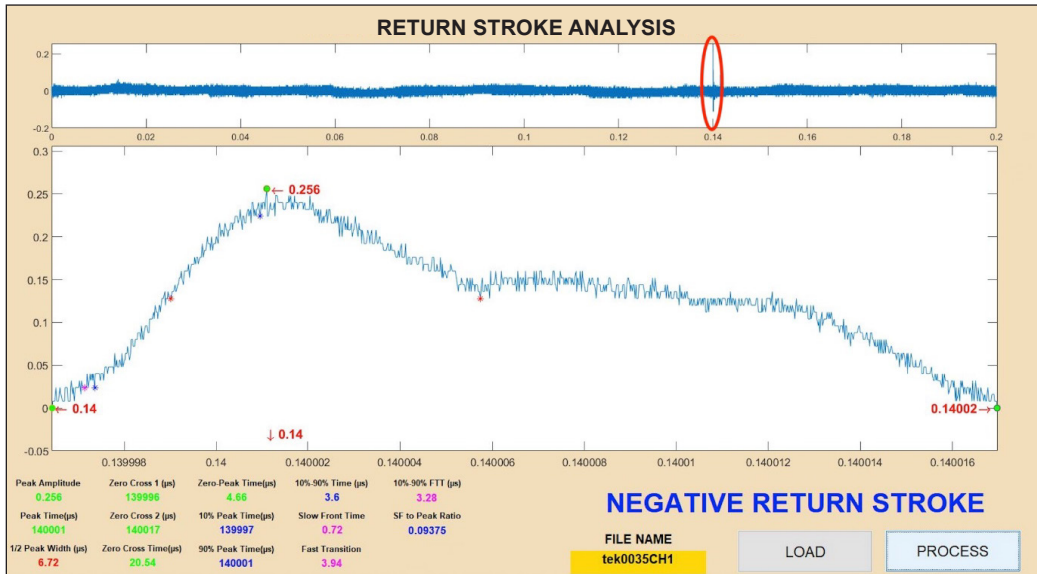

Figure 14. GUI of output waveform spectrum and analysed negative return strokes

CONCLUSIONS

This study demonstrated an automated negative lightning return strokes characterization based on seven main parameters using the brute-force search algorithm and MATLAB software. A total of 170 lightning electric field signals were recorded and characterized automatically using the algorithm. The algorithm's working principle operated based on the comparative search concept, time-reversal search concept, and time forward concept. These concepts provided an effective method for characterizing negative lightning return strokes, mainly on the seven parameters in this study. Based on the data comparison between this study's manual and automated data, a small difference between the two data measurements was observed. The percentage difference range was less than 5%, which was between 1.19% and 4.82%. The AM and SD for the automated data were also consistent with the manual data. Furthermore, most of the plotted data were within the upper and lower limits of agreement, as evident from the Bland-Altman graphs. Overall, the results of the statistical approach that involved analysis on the percentage difference, AM, SD, and Bland-Altman plots demonstrated the capability of the proposed algorithm in the characterization of negative lightning return strokes parameters. In particular, the algorithm development

provided a practical and feasible method to analyze and characterize the related parameters with a faster processing time and optimize the characterization accuracy. For future work, the implementation of artificial intelligence, which involves training, testing, and validating the data set of the lightning-generated electric field powered by machine learning or deep learning, could improvise the algorithm's accuracy.

ACKNOWLEDGEMENTS

REFERENCES

Ahmad, N. A., Fernando, M., Baharudin, Z. A., Cooray, V., Ahmad, H., & Malek, Z. A. (2010). Characteristics of narrow bipolar pulses observed in Malaysia. *Journal of Atmospheric and Solar-Terrestrial Physics, 72*(5-6), 534-540. https://doi.org/10.1016/j.jastp.2010.02.006

Arshad, S. A. M. (2017). *Characterization of lightning-generated electric fields and development of automated measuring system for cloud-to-ground lightning in Malaysia* (Doctoral dissertation). Universiti Putra Malaysia, Malaysia. http://psasir.upm.edu.my/id/eprint/70239.

Beasley, W. (1985). Positive cloud-to-ground lightning observations. *Journal of Geophysical Research: Atmospheres, 90*(D4), 6131-6138. https://doi.org/10.1029/JD090iD04p06131

Chi, G., Zhang, Y., Zheng, D., Lu, W., & Zhang, Y. (2014). Characteristics of lightning activities in Potala Palace region of Tibet. In *2014 International Conference on Lightning Protection (ICLP)* (pp. 1992-1994). IEEE Publishing. https://doi.org/10.1109/ICLP.2014.6973455.

Chum, C. S., Jun, C., & Zhang, X. (2014). Implementation of randomize-then-combine constructed hash function. In *2014 23rd Wireless and Optical Communication Conference (WOCC)* (pp. 1-6). IEEE Publishing. https://doi.org/10.1109/WOCC.2014.6839925

Cikač, D., Turk, N., Bulić, N., & Barbanti, S. (2020). Pulse pattern optimization based on brute force method for medium-voltage three-level npc converter with active front end. *Electronics, 9*(10), Article 1685. https://doi.org/10.3390/electronics9101685

Cooray, V. (2003). The mechanism of the lightning flash. In *The lightning flash* (pp. 127-240). The Institution of Engineering and Technology. https://doi.org/10.1049/PBPO069E

Cooray, V., & Lundquist, S. (1985). Characteristics of the radiation fields from lightning in Sri Lanka in the tropics. *Journal of Geophysical Research: Atmospheres, 90*(D4), 6099-6109. https://doi.org/10.1029/JD090iD04p06099

Cooray, V. (2014). Mechanism of the lightning flash. In *The lightning flash* (pp. 119-229). The Institution of Engineering and Technology. https://doi.org/10.1049/PBPO069E_ch4

Cooray, V. (2015). *An introduction to lightning*. Springer. https://doi.org/10.1007/978-94-017-8938-7

Cooray, V., & Lundquist, S. (1982). On the characteristics of some radiation fields from lightning and their possible origin in positive ground flashes. *Journal of Geophysical Research: Oceans, 87*(C13), 11203-11214. https://doi.org/10.1029/jc087ic13p11203

Davidrajuh, R., & Rong, C. (2019). Solving scheduling problems with randomized and parallelized brute-force approach. In *2019 Computer Science and Information Technologies (CSIT)* (pp. 1-4). IEEE Publishing. https://doi.org/10.1109/CSITechnol.2019.8895104

Dwyer, J. R., & Uman, M. A. (2014). The physics of lightning. *Physics Reports, 534*(4), 147-241. https://doi.org/10.1016/j.physrep.2013.09.004

Gomes, C., Cooray, V., & Ab Kadir, M. Z. A. (2013). Vertical electric fields and field change parameters due to partly inclined lightning leader channels. *Progress In Electromagnetics Research, 135*, 55-80. https://doi.org/10.2528/PIER12081809

Gomes, C., Cooray, V., & Jayaratne, C. (1998). Comparison of preliminary breakdown pulses observed in Sweden and in Sri Lanka. *Journal of Atmospheric and Solar-Terrestrial Physics, 60*(10), 975-979. https://doi.org/10.1016/S1364-6826(98)00007-8

Haddad, M. A., Rakov, V. A., & Cummer, S. A. (2012). New measurements of lightning electric fields in Florida: Waveform characteristics, interaction with the ionosphere, and peak current estimates. *Journal of Geophysical Research Atmospheres, 117*(D10). https://doi.org/10.1029/2011JD017196

Hamzah, M. N. (2015). *Distinct characteristics of cloud-to-ground lightning electric fields generated in Malaysia* (Masters dissertation). Universiti Putra Malaysia, Malaysia. http://psasir.upm.edu.my/id/eprint/56237

Hazmi, A., Emeraldi, P., Hamid, M. I., & Takagi, N. (2017). Research on positive narrow bipolar events in Padang. In *2016 3rd International Conference on Information Technology, Computer, and Electrical Engineering (ICITACEE)* (pp. 156-159). IEEE Publishing. https://doi.org/10.1109/ICITACEE.2016.7892429

Heidler, F., & Hopf, C. (1998). Measurement results of the electric fields in cloud-to-ground lightning in nearby Munich, Germany. *IEEE Transactions on Electromagnetic Compatibility, 40*(4), 436-443. https://doi.org/10.1109/15.736204

Hojo, J., Ishii, M., Kawamura, T., Suzuki, F., & Funayama, R. (1985). The fine structure in the field change produced by positive ground strokes. *Journal of Geophysical Research: Atmospheres, 90*(D4), 6139-6143. https://doi.org/10.1029/JD090iD04p06139

Hyndman, R. J., & Koehler, A. B. (2006). Another look at measures of forecast accuracy. *International Journal of Forecasting, 22*(4), 679-688. https://doi.org/10.1016/j.ijforecast.2006.03.001

Ibrahim, W. I., Ghazali, M. R., Ghani, S. A., & Malek, Z. A. (2011). Measurement of vertical electric fields from lightning flashes using parallel plate antenna. In *International Conference On Electrical, Control And Computer Engineering 2011 (INECCE)* (pp. 466-471). IEEE Publishing. https://doi.org/10.1109/INECCE.2011.5953927

Idone, V. P., & Orville, R. E. (1982). Lightning return stroke velocities in the thunderstorm research international program (TRIP). *Journal of Geophysical Research: Oceans, 87*(C7), 4903-4916. https://doi.org/10.1029/jc087ic07p04903

Ishii, M., & Hojo, J. I. (1989). Statistics on fine structure of cloud-to-ground lightning field waveforms. *Journal of Geophysical Research: Atmospheres, 94*(D11), 13267-13274. https://doi.org/10.1029/jd094id11p13267

Klaver, T. P. C., Simonovic, D., & Sluiter, M. H. F. (2018). Brute force composition scanning with a CALPHAD database to find low temperature body centered Cubic High Entropy alloys. *Entropy, 20*(12), Article 911. https://doi.org/10.3390/e20120911

Master, M. J., Uman, M. A., Beasley, W., & Darveniza, M. (1984). Lightning induced voltages on power lines: Experiment. *IEEE Transactions on Power Apparatus and Systems, PAS-103*(9), 2519-2529. https://doi.org/10.1109/TPAS.1984.318406

Miller, B. N., & Ranum, D. L. (2011). *Problem solving with algorithms and data structures using python* (2nd Ed.). Franklin, Beedle & Associates Inc.

Nag, A., & Rakov, V. A. (2014). Parameters of electric field waveforms produced by positive lightning return strokes. *IEEE Transactions on Electromagnetic Compatibility, 56*(4), 932-939. https://doi.org/10.1109/TEMC.2013.2293628

Orville, R. E. (1968). A high-speed time-resolved spectroscopic study of the lightning return stroke: Part I. A qualitative analysis. *Journal of the Atmospheric Sciences, 25*(5), 827-838. https://doi.org/10.1175/1520-0469(1968)025<0827:ahstrs>2.0.co;2

Raafat, S. M., & Naji, D. J. (2018). Intelligent optimized controlled health care system using brute force and heuristic algorithms. In *2018 Third Scientific Conference of Electrical Engineering (SCEE)* (pp. 134-139). IEEE Publishing. https://doi.org/10.1109/SCEE.2018.8684216

Rakov, V. A. (2016). *Fundamentals of lightning*. Cambridge University Press. https://doi.org/10.1017/cbo9781139680370

Robinson, A. C., & Quinn, S. D. (2018). A brute force method for spatially-enhanced multivariate facet analysis. *Computers, Environment and Urban Systems, 69*, 28-38. https://doi.org/10.1016/j.compenvurbsys.2017.12.003

Santamaría, F., Gomes, C., & Roman, F. (2006). Comparison between the signatures of lightning electric field measured in Colombia and that in Sri Lanka. In *Proceedings of the 28th International Conference on Lightning Protection* (pp. 254-256). ICLP Publishing. https://doi.org/10.14936/ieiej.27.226

Sharma, S. R., Fernando, M., & Gomes, C. (2005). Signatures of electric field pulses generated by cloud flashes. *Journal of Atmospheric and Solar-Terrestrial Physics, 67*(4), 413-422. https://doi.org/10.1016/j.jastp.2004.09.007

Sudin, S. (2019). *Performance prediction based on fitness level for track cycling activity using artificial intelligence* (Doctoral dissertation). Universiti Malaysia Perlis, Malaysia.

Thike, A. M., Lupin, S., & Vagapov, Y. (2017). Implementation of brute force algorithm for topology optimisation of wireless networks. In *2016 International Conference for Students on Applied Engineering (ICSAE)* (pp. 264-268). IEEE Publishing. https://doi.org/10.1109/ICSAE.2016.7810200

Weidman, C. D., & Krider, E. P. (1978). The fine structure of lightning return stroke wave forms. *Journal of Geophysical Research: Oceans, 83*(C12), 6239-6247. https://doi.org/10.1029/jc083ic12p06239

Wooi, C. L., Abdul-Malek, Z., Ahmad, N. A., & El Gayar, A. I. (2016). Statistical analysis of electric field parameters for negative lightning in Malaysia. *Journal of Atmospheric and Solar-Terrestrial Physics, 146*, 69-80. https://doi.org/10.1016/j.jastp.2016.05.007

Willett, J. C., & Krider, E. (2000). Rise times of impulsive high-current processes in cloud-to-ground lightning. *IEEE Transactions on Antennas and Propagation, 48*(9), 1442-1451. https://doi.org/10.11090/8.898779.